HYDROPHOBIC ZNFE2O4 MAGNETIC NANOPARTICLES WITH WELL-DEFINED SUPERBALL MORPHOLOGY AND ROOM-TEMPERATURE SUPERPARAMAGNETISM

DOI: 10.66951/PHIO6007; https://doi.org/10.66951/PHIO6007

Štefan Hricov, stefan.hricov@matfyz.cuni.cz
Department of Condensed Matter Physics, Faculty of Mathematics and Physics, Ke Karlovu 5, 121 16 Prague, Czechia

Dominika Zákutná, zakutnad@ill.fr
Institut Laue-Langevin - The European Neutron Source, 71 avenue des Martyrs, 38042 Grenoble, France

Jana Vejpravová, jana.vejpravova@matfyz.cuni.cz
Department of Condensed Matter Physics, Faculty of Mathematics and Physics, Ke Karlovu 5, 121 16 Prague, Czechia

Veronika Gajdošová, gajdosova@imc.cas.cz
Department of Polymer Morphology, Institute of Macromolecular Chemistry CAS, Heyrovského nám. 2, 162 00 Prague, Czechia

Abstract

For fundamental and applicative research, narrowly size-distributed magnetic nanoparticles are essential for drawing reliable correlations between structure and properties. Here, we report a robust synthesis protocol for $ZnFe_2O_4$ magnetic nanoparticles based on the thermal decomposition of metal-organic salts in the presence of oleic acid as a surfactant, performed in a high-boiling-point solvent. The morphological quality and size distribution of resulting nanoparticles were assessed by transmission electron microscopy and image analysis. Complementary characterization by powder X-ray diffraction and DC magnetometry provided insight into their structural and magnetic properties.

1 Introduction

Size-related effects provide a key access window into novel properties of materials, often contrasting with their bulk counterparts. In this context, the advent of magnetic nanoparticles (MNPs) research unravelled unprecedented applicative potential of this particular class of materials. MNPs are already in use or proposed to be implemented in hyperthermia cancer treatment[1,2], bio-imaging[3,4], spintronics[5] or catalysis[6]. Particularly, thanks to their excellent chemical stability, the ferrites are the subject of a sustained research interest over the years[7,8]. While the illustrious magnetite nanoparticles have received noticeable attention, due to their magnetic properties[9] and excellent biocompability[10], for an appropriate material selection designated for commercial use, a broad spectrum of deeply studied entries must be available. Therefore, among the comparatively underinvestigated ferrite MNPs are, for example, the $ZnFe_2O_4$ MNPs. In its bulk form, $ZnFe_2O_4$ possesses normal spinel structure and antiferromagnetic ordering below the Néel temperature ($T_N \approx 10$ K)[11]. However, as MNPs, $ZnFe_2O_4$ exhibits either ferrimagnetic or superparamagnetic behavior, depending on a given temperature regime[12]. To obtain $ZnFe_2O_4$ MNPs, various synthesis procedures were employed, such as co-precipitation[13] or synthesis under solvothermal conditions[14].

For adequate properties evaluation, it is essential to be able to fabricate $ZnFe_2O_4$ MNPs with narrow size distribution and well-defined morphology. To achieve this goal, we synthesize $ZnFe_2O_4$ via

thermal decomposition using high boiling point solvent. Morphological evaluation of resulting products was carried out using transmission electron microscopy (TEM), accompanied by respective image analysis with reconstructed size distribution. Moreover, to confirm presence of $ZnFe_2O_4$ phase, powder X-ray diffraction (PXRD) was performed. The diffraction pattern was analyzed using full-profile Rietveld refinement. Information about the sample's texture was further retrieved by employing spherical harmonics within the full-profile analysis. As for magnetic properties, the DC magnetometry was utilized resulting in ZFC-FC and several isothermal hysteresis loops.

2 Experimental

2.1 Synthesis of $ZnFe_2O_4$ nanoparticles

Iron(III) acetylacetonate (97%), zinc(II) acetylacetonate (99.995%), oleic acid (90%) and 1-octadecene (90%) dibenzylether (98%) were purchased from Sigma Aldrich, acetone (99.5%) and ethylacetate (≥ 99.5%) from VWR and finally ethanol (98%) from Penta Chemicals. $ZnFe_2O_4$ MNPs were prepared via thermal decomposition of organic metal salts. At first, 1.26 mmol of $Zn(acac)_2$ and

2.56 mmol of $Fe(acac)_3$ was weighed into a 50mL three-neck round bottom flask, followed by addition of 15.6 mmol of oleic acid (OA). Subsequently, 5 mL of 1-octadecene and dibenzylether was added and the reaction mixture was left to dissolve at 60 °C for 15 min under flowing N_2. The flask was placed into the heating mantle, and heating profile was started – first, the reaction was heated up to 290 °C at a heating rate of 7.67 °C/min. Subsequently, a 1-hour plateau was maintained at this temperature. After the reaction ended, the 50mL three-neck round-bottom flask was removed from the heating mantle and allowed to cool down under ambient conditions. For the purpose of purification, the whole volume of reaction mixture was transferred into a 50mL Falcon® tube. Residual product remaining inside the round-bottom flask was washed out using *approx.* 5 mL of toluene. Furthermore, *approx.* 20 ml of reaction mixture were evenly divided in total among four 50mL Falcon® test tubes. Then, into each one of them, 10 mL of iPrOH, 8 mL of EtOAc and 2 mL of EtOH were added. Solvent addition was followed by centrifugation at 7830 RPM (6511 g) for 30 min. The resulting dark-colored opaque supernatant was discarded, and pellets were redispersed in 5 mL of toluene. Eventually, 5 mL of iPrOH, 4 mL of EtOAc and 1 mL of EtOH were added to the redispersed MNPs and centrifuged at 7830 RPM (6511 g) for 10 min. Transparent, brownish supernatant was discarded, MNPs were redispersed in 5 mL of toluene and collected.

3 Results and Discussion

3.1 Transmission electron microscopy

Morphological evaluation was performed by transmission electron microscopy (TEM), utilizing a Tecnai G2 Spirit microscope from FEI operating at 120 kV. Bright-field micrographs (**Figure 1A, 1B)** reveal a well-defined superball morphology with a high degree of the shape uniformity. To determine the size distribution of MNPs system, image analysis was performed on the micrographs and the resulting histogram, (**Figure 1C)**, was fitted with a log-normal function, yielding a mean particle diameter of d_{TEM} = 18.32(6) nm and a polydispersity of 8.2(3) %, indicating narrowly distributed, monodisperse system.

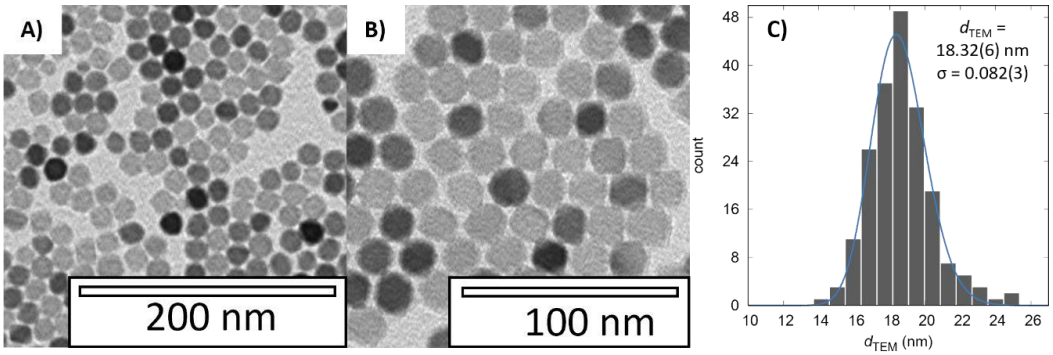


Figure 1. A) TEM-BF micrograph of ZnFe2O4 MNPs Detailed look on MNPs is on a zoomed micrograph, B). C) size distribution with fitted log-normal function, obtained from the image analysis of TEM BF micrographs.

3.2 Powder X-ray diffraction

Phase composition was confirmed by PXRD using a Panalytical X'pert Pro diffractometer equipped with Cu K_α radiation. Observed diffraction pattern was analyzed by full-profile Rietveld refinement in WinPLOTR (FullProf suite [15,16]), incorporating SPHR texture refinement to extract directional crystallite size parameters. Contributions from instrumental broadening were accounted for by calculating instrumental resolution function, based on the LaB_6 diffraction pattern. The refined pattern (**Figure 2A)** confirms the spinel $ZnFe_2O_4$ phase with no detectable impurities. From the Lorentzian broadening, an apparent crystallite size of d_{PXRD} = 14.6(7) nm was obtained, which is notably smaller than d_{TEM}. This discrepancy indicates that the coherently scattering domain does not extend to the full physical boundary of nanoparticles, consistent with the structural disorder in the near-surface layers, as commonly observed in nanoscale system. Independently, the crystallite shape reconstructed from the SPHR refinement (**Figure 2B**) is consistent with superball morphology identified by TEM, providing corroborating evidence for the morphological uniformity of the sample. To emphasize direction- dependent size parameters retrieved from the SPHR refinement, one may consider **(Figure 2C)** with illustrative directional indicators.

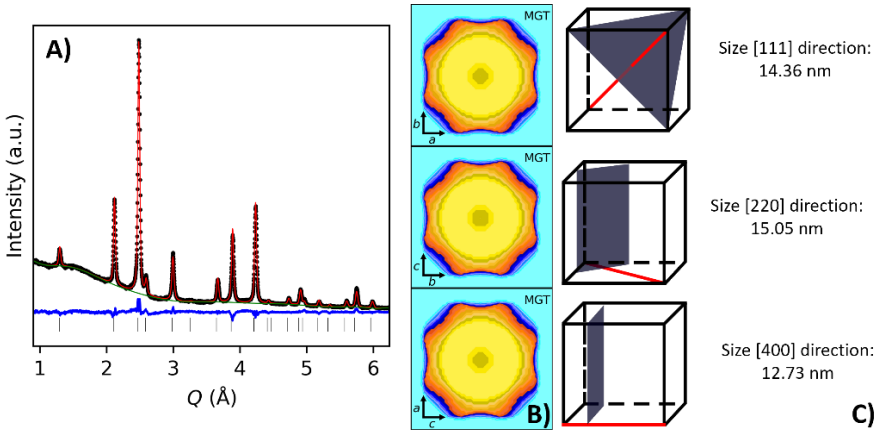


Figure 2. A) PXRD of MNPs with SPHR fit, where black dots represent observed intensity, red curve calculated pattern, green curve a background function (Chebyshev polynomials) and the blue curve is difference between calculated and observed intensity. Diffraction maxima of ZnFe2O4 phase are depicted as black vertical lines. B) Average crystallite shape is accompanying the diffraction pattern. C) Direction-dependent size parameters are shown alongside the corresponding schematic direction indicators.

3.3 Magnetic measurements

To prepare powder sample, the MNPs toluene dispersion was dried in a watch glass and homogenized in a mortar. A 7.7 mg aliquot was loaded into a Vibrating Sample Magnetometry (VSM) powder sample capsule, fixed with cyanoacrylate adhesive, and measured on the physical property measurement system (PPMS) from Quantum Design equipped with VSM module. The ZFC/FC magnetization curves, measured under an applied magnetic field of 10 mT are shown in **(Figure 3A).** The blocking temperature, T_B was estimated from the peak in the temperature derivative of the ZFC – FC magnetization difference **(Figure 3B)** yielding $T_B \approx 19$ K. A series of isothermal hysteresis loops recorded at selected temperatures, **(Figure 3D)**, clearly shows progressive increase in saturation magnetization upon cooling, consistent with enhanced spin alignment. Moreover, at 3 K and below T_B, the MNPs reside in the blocked state and exhibit a ferrimagnetic response, evidenced by a weak but finite coercivity of $\mu_0 H_c = 21$ mT. To probe for a potential exchange bias arising from pinned surface magnetic moments, the sample was field-cooled to 3 K under 7T applied field and a subsequent hysteresis loop was recorded **(Figure 3D)**. The FC hysteresis loop shows no horizontal shift, $\mu_0 H_c =$ 21 mT remaining identical to its zero-field-cooled counterpart, unambiguously ruling out exchange-bias contribution.

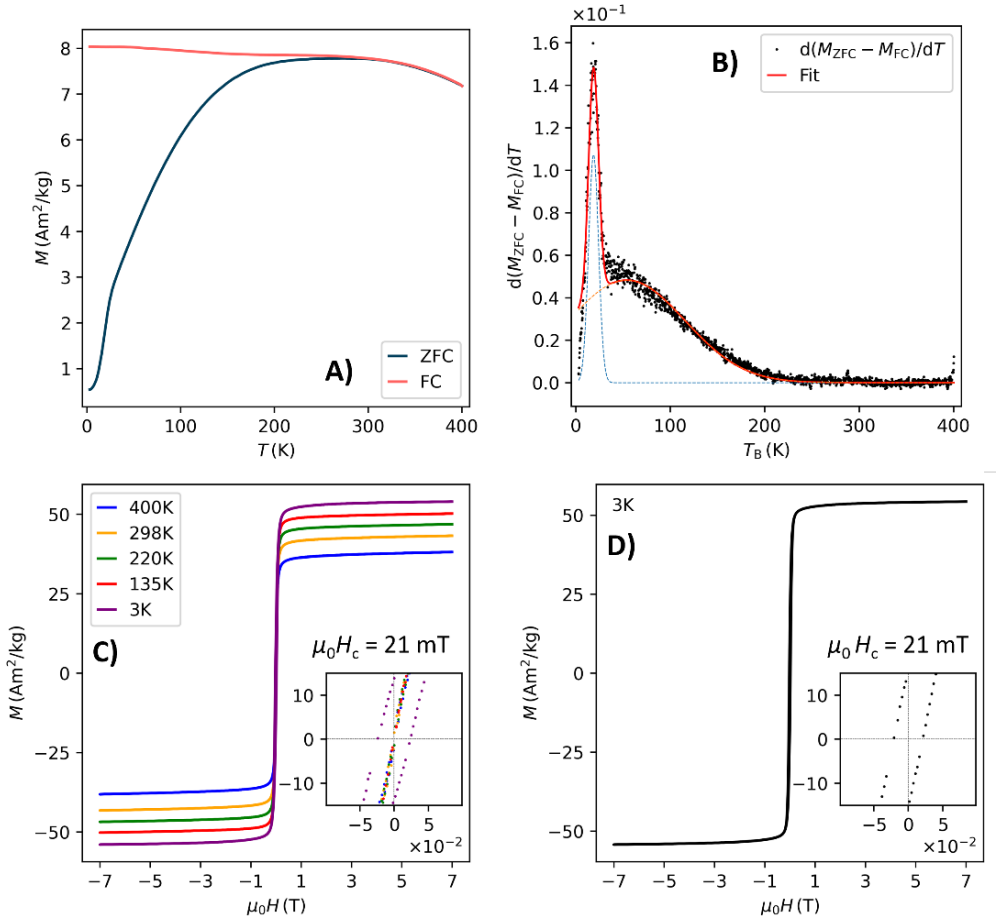


Figure 3. A) ZFC-FC temperature dependent magnetization measurement, B) temperature ZFC-FC magnetization difference derivative with estimated *T*B, C) series of isothermal hysteresis loops with zoomed inset for coercivity evaluation and D) FC-hysteresis (7 T cooling field, 3 K) with zoomed inset.

4 Summary

To fabricate monodisperse and morphologically well-developed superball $ZnFe_2O_4$ MNPs, the thermal decomposition of metal-organic salts in a high-boiling-point solvent was utilized. MNPs, with a size of 18.32(6) nm and polydispersity of 8.2(3) % were obtained. To confirm presence of $ZnFe_2O_4$ phase, the PXRD pattern was recorded and subsequently analyzed by full-profile analysis. Magnetic

characterization unveiled low $T_B \approx 19$ K together with minuscule $\mu_0 H_c = 21$ mT recorded at 3 K. Moreover, the FC-hysteresis disproves pinning of magnetic moments within the MNPs. Taken together, these results demonstrate that the synthesized $ZnFe_2O_4$ MNPs exhibit robust room-temperature superparamagnetic, defining property that makes this system attractive for biomedical and technological applications where a magnetically switchable, remanence-free response is required. Given the relative scarcity of well-characterized $ZnFe_2O_4$ systems in the literature compared to magnetite, this work provides a reproducible synthetic benchmark and a complete structural–magnetic property profile against which future studies can be referenced.

5 Acknowledgement

This work has been funded by a grant from the Programme Johannes Amos Comenius under the Ministry of Education, Youth and Sports of the Czech Republic CZ.02.01.01/00/22_008/0004558 Advanced MUltiscaLe materials for key Enabling Technologies.

6 References

[1] M. Lin, J. Huang, and M. Sha, Recent Advances in Nanosized Mn-Zn Ferrite Magnetic Fluid Hyperthermia for Cancer Treatment, Journal of Nanoscience and Nanotechnology **14**, 792 (2014).

[2] E. Mazario, N. Menéndez, P. Herrasti, M. Cañete, V. Connord, and J. Carrey, Magnetic Hy- perthermia Properties of Electrosynthesized Cobalt Ferrite Nanoparticles, American Chemical Society **117**, 11405 (2013).

[3] J. Estelrich, M. J. Sánchez-Martín, and M. A. Busquets, Nanoparticles in magnetic resonance imaging: from simple to dual contrast agents, International Journal of Nanomedicine **10**, 1727 (2015).

[4] K.-S. Kim, J.-H. Han, J.-H. Park, H.-K. Kim, S. H. Choi, G. R. Kim, H. Song, H. J. An, D. K. Han, W. Park, and K.-S. Park, Multifunctional nanoparticles for genetic engineering and bioimaging of natural killer (NK) cell therapeutics, Biomaterials **221**, 119418 (2019).

[5] Q. K. Ong, X.-M. Lin, and A. Wei, Role of Frozen Spins in the Exchange Anisotropy of Core-Shell Fe@Fe3O4 Nanoparticles, J. Phys. Chem. C **115**, 2665 (2011).

[6] L. M. Rossi, N. J. S. Costa, F. P. Silva, and R. Wojcieszak, Magnetic nanomaterials in catalysis: advanced catalysts for magnetic separation and beyond, Green Chem., **16**, 2906–2933 (2014).

[7] Y. Ichiyanagi, M. Kubota, S. Moritake, Y. Kanazawa, T. Yamada, and T. Uehashi, Magnetic properties of Mg-ferrite nanoparticles, J. Magn. Magn. Mat., **310**, 2378–2380 (2007).

[8] A. López-Ortega, E. Lottini, C. de J. Fernández, and C. Sangregorio, Exploring the Magnetic Properties of Cobalt-Ferrite Nanoparticles for the Development of a Rare-Earth-Free Permanent Magnet, Chem. Mater., **27**, 4048–4056 (2015).

[9] Y. Wei, B. Han, X. Hu, Y. Lin, X. Wang, and X. Deng, Synthesis of Fe3O4 Nanoparticles and their Magnetic Properties, Procedia Eng., **27**, 632–637 (2012).

[10] P. Figueiredo, K. Lintinen, A. Kiriazis, V. Hynninen, Z. Liu, T. Bauleth-Ramos, A. Rahikkala, A. Correia, T. Kohout, B. Sarmento, J. Yli-Kauhaluoma, J. Hirvonen, O. Ikkala, M. Kostiainen, and H. Santos, In vitro evaluation of biodegradable lignin-based nanoparticles for drug delivery and enhanced antiproliferation effect in cancer cells, Biomaterials, **121**, 97–108 (2017).

[11] J. Gass, H. Srikanth, N. Kislov, S. Srinivasan, and Y. Emirov, Magnetization and magnetocaloric effect in ball-milled zinc ferrite powder, J. Appl. Phys., **103**, 07B309 (2008).

[12] V. Blanco-Gutierrez, E. Climent-Pascual, M. Torralvo-Fernandez, R. Saez-Puche, and M. Fernandez-Diaz, Neutron diffraction study and superparamagnetic behavior of $ZnFe_2O_4$ nanoparticles obtained with different conditions, J. Solid State Chem., **184**, 1608–1613 (2011).

[13] R. Haghniaz, A. Rabbani, F. Vajhadin, T. Khan, R. Kousar, A. Khan, H. Montazerian, J. Iqbal, A. Libanori, H.J. Kim, and F. Wahid, Antibacterial and wound healing-promoting effects of zinc ferrite nanoparticles, J. Nanobiotechnology, **19**, 38 (2021).

[14] P. Lyu, Y. Hou, R. Wang, M. Ma, Y. Chen, Q. Xing, Y. Ma, S. Wang, Y. Wu, and W. Huang, Synthesis of $ZnFe_2O_4$@Mg-Al-SDBS LDH composites for regulating heat and fire safety properties of polyurea, Polym. Adv. Technol., **33**, 4290–4301 (2022).

[15] J. Rodríguez-Carvajal, Recent advances in magnetic structure determination by neutron powder diffraction., Physica B: Condensed Matter, **192**, 55-69 (1993).

[16] T. Roisnel, J. Rodríguez-Carvajal, WinPLOTR: a Windows tool for powder diffraction patterns analysis, Materials Science Forum, Proceedings of the Seventh European Powder Diffraction Conference (EPDIC 7), 118-123 (2000).